J. Biomechanics Vol. 26, No. 9, pp. 1091–1104, 1993.
Printed in Great Britain

0021–9290/93 $6.00+.00

BIOMECHANICAL MODEL OF THE HUMAN FOOT: KINEMATICS AND KINETICS DURING THE STANCE PHASE OF WALKING

STEPHEN H. SCOTT*† and DAVID A. WINTER‡§

*Department of Systems Design Engineering; and ‡Department of Kinesiology, University of Waterloo, Waterloo, Ontario N2L 3G1, Canada

Abstract—A model of the human foot is proposed in which the foot is represented as eight rigid segments and eight monocentric, single-degree-of-freedom joints. The soft tissue under the foot is divided into seven independent sites of contact, or loading, and each of these is modelled as a nonlinear spring and a nonlinear damper in-parallel. The model was used to estimate the kinematics and kinetics of the foot during the stance phase of walking. The force sustained at each loading site was calculated from walking trials in which only portions of the foot landed on a small force platform. The position of the calcaneus was defined by surface markers, whereas the position of the distal segments were based upon chalk footprints and an estimate of the compression of the plantar soft tissue. The results suggest that the joints that constitute the longitudinal arch extend slightly when the forefoot is loaded. During push-off, these joints flex as the metatarsophalangeal joints extend. Similar kinematic results were estimated when the distal segments of the foot were defined by surface markers. The magnitude of the joint moments of force depended largely on the distribution of the load under the foot which varied considerably between subjects. The stable, yet resilient properties of the foot, as highlighted by this model, should be considered in three-dimensional dynamic models used to study human locomotion. The model provides an objective tool to quantify foot motion and loading, which may prove useful for describing foot function in normal and pathological conditions.

NOTATION

P_i	position coordinate of segment i in the global coordinate system
p_i	position coordinate of segment i in a local coordinate system
$[\ ]_i$	position vector in local coordinate system i
$[M]_{ij}$	transformation matrix from i to j coordinate systems

NOMENCLATURE

F_p	soft-tissue force
j, k, l, m, n	constants for soft-tissue model
ε	soft-tissue strain
$\dot{\varepsilon}$	soft-tissue strain rate
Q	thickness of soft tissue
1	first metatarsal
2	mid-tarsal segment
3	third metatarsal
4	fourth metatarsal
5	fifth metatarsal
6	hallux
c	calcaneus
δ	radius of metatarsal head
α_i	rotation of joint i
1T	first tarsometatarsal joint
2T	second tarsometatarsal joint
3T	third tarsometatarsal joint
4T	fourth tarsometatarsal joint
5T	fifth tarsometatarsal joint
CP	center of pressure
CP^{pred}	estimated center of pressure from summation of GRF_i
G	global reference system
GRF	ground reaction force
GRF_i	ground reaction force at the ith point of contact
GRF^{pred}	summation of GRF_i at all points of contact
LRS	local reference system
MP	metatarsophalangeal joint
TC	talocrural joint
TCN	talocalcaneal joint
TT	transverse tarsal joint

Received in final form 8 *December* 1992.

†Present Address: Centre de recherche en sciences neurologiques (CRSN), Département de physiologie, Faculté de médecine, Université de Montréal, C.P. 6128, succursale A, Montréal (Quebec) H3C 3J7, Canada.

§Author to whom correspondence should be addressed.

INTRODUCTION

Mechanical analyses of human movement have improved the understanding of how we generate and control limb movement. The vast majority of these studies have used inverse dynamical techniques; neural and motor (forces and moments) patterns are estimated based on information on actual human movement and a mathematical representation of the body. An alternate technique, often called the forward or direct dynamics solution, takes a mathematical representation of the body and simulates a movement based on some neural or motor pattern. Many researchers have developed dynamic models to simulate human locomotion (Beckett and Chang, 1968; Chow and Jacobson, 1971; Chen *et al.*, 1986; Mochon and McMahon, 1980; Onyshko and Winter, 1980; Pandy and Berme, 1988; Siegler *et al.*, 1982), but these models have been largely restricted to two-dimensional representations due to the complexity and

computational costs of the equations and the difficulty in controlling multisegmental models. One of the most difficult problems with these models is their interaction with the environment. For locomotion, this pivotal role is performed by the foot, which has probably been the most poorly modelled portion of the lower limb. In general, previous models have assumed that the foot has no toes, any joints distal to the ankle, any viscoelastic plantar tissue, nor any spatial characteristics in the mediolateral axis. The inaccuracy of the foot model is demonstrated by the large discrepancy between the predicted power flows in and out of this structure, and its rate of change of mechanical energy (Robertson and Winter, 1980). With recent improvements in computer systems and software, three-dimensional models of the human body are being realized, but they will require extensive improvement in the structure of the foot.

In defense of the assumptions used in these models, the literature provides little quantitative data on the kinetics and kinematics of foot motion during walking. Classical analysis of foot function has relied largely on qualitative assessments (Burns, 1987; Hamilton and Ziemer, 1981; Klenerman, 1982; Mann, 1986). A model-based approach has been used to analyze foot function (Proctor and Paul, 1982; Scott and Winter, 1991; Salathé *et al.*, 1986; Snijders *et al.*, 1986; Stokes *et al.*, 1979; Wyss *et al.*, 1990). However, these models have analyzed only one or a few of the joints within the foot and have not attempted to model the foot in its entirety. A six segment model of the foot has been presented recently (Morlock and Nigg, 1991), but was not developed, nor used, to study foot function during walking. The purpose of this investigation was (1) to develop a model of the human foot based upon its anatomical structure, and (2) to use the model to estimate the joint kinematics and kinetics of the foot during the stance phase of walking. The synthesis of this model and the measurement of the mechanics of the foot during locomotion provide a crucial step in the development of a three-dimensional model of the human body. Since the structure of the model was based upon the anatomy of the foot, the model and results may prove useful for other related research and clinical fields. Knowledge on the mechanical behavior of the foot is required by orthopeadic surgeons and podiatrists in order to understand the implications that surgical and nonsurgical interventions may have on this complex structure (Mann, 1986). The model may also prove to be useful for describing foot function in fields such as sports medicine, although the suitability of the model must be re-evaluated for each individual situation.

THE MODEL

The proposed foot model consists of eight segments and eight monocentric, single-degree-of-freedom hinge joints (Fig. 1). The plantar soft tissue was modelled as a set of seven springs and dampers in-parallel. The talus and the calcaneus were each modelled as rigid bodies. The talocrural (ankle) joint provides rotation between the talus and the leg, and the talocalcaneal (subtalar) joint provides rotation between the talus and the calcaneus (Hicks, 1953; Isman and Inman, 1969). Anatomical studies suggest that the talocalcaneal joint does not act as a hinge joint (Engsberg, 1987; Langelaan, 1983; Siegler *et al.*, 1988), but a recent study has found that the angular motion of this joint during walking can be represented adequately by a single-degree-of-freedom, monocentric joint (Scott and Winter, 1991). Therefore, both the talocrural and the talocalcaneal joints were modelled as simple hinge joints. The analysis of the kinetics and kinematics of these joints during the stance phase of walking have already been reported in a recent paper (Scott and Winter, 1991) and will not be discussed further.

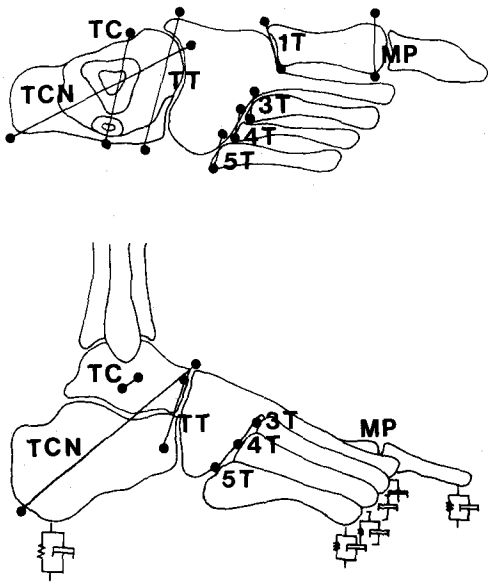

Fig. 1. Dorsal and lateral view of the proposed model of the human foot consisting of eight rigid segments and eight monocentric single-degree-of-freedom joints. The soft tissue was divided into seven separate structures each modelled as a nonlinear spring and nonlinear damper in-parallel. The seventh spring and damper, under the head of the first metatarsal, is obscured from the lateral view. Joint acronyms: TC-talocrural, TCN-talocalcaneal, TT-transverse tarsal, 1T-1st tarsometatarsal, 3T-3rd tarsometatarsal, 4T-4th tarsometatarsal, 5T-5th tarsometatarsal, MP-metatarsophalangeal.

The intertarsal joints other than the talocalcaneal joint have received little attention in the literature. Motion between the hind- and mid-foot regions occurs at the transverse tarsal (mid-tarsal) joint (Elftman, 1960; Hicks, 1953; Mann, 1982; Manter, 1941; Ouzounian and Shereff, 1989). This joint is actually created by two separate joints, the talonavicular and the calcaneocuboid joints. Its axis passes through the foot in a medial, anterior and superior direction (TT in

Fig. 1). The other intertarsal joints have flat articulating surfaces, but a tight ligamentous structure surrounds these joints so that little motion is permitted (Klenerman, 1982). These joints have been recently shown to provide some motion, but the range is generally smaller than the transverse tarsal (Ouzounian and Shereff, 1989). The model included the transverse tarsal joint and assumed that a rigid mid-tarsal segment was created by the navicular, the cuboid and the three cuneiform bones.

Limited motion occurs between the distal tarsal and the five metatarsal bones. The greatest range of motion has been considered to occur between the first cuneiform and the first metatarsal bone (Burns, 1987; Hicks, 1953; Hamilton and Ziemer, 1981; Klenerman, 1982) although others suggest that little motion occurs at this joint (Wanivenhaus and Pretterklieber, 1989). A study by Ouzounian and Shereff (1989) demonstrated that the greatest range of motion is between the cuboid and fourth metatarsal and between the cuboid and the fifth metatarsal. Motion between the tarsal and the second metatarsal bones is the most limited because this metatarsal bone has a firm socket attachment to all three cuneiform bones (Hamilton and Ziemer, 1983; Moore, 1985; Ouzounian and Shereff, 1989; Riegger, 1988). The increased stability of the second tarsometatarsal joint is necessary in late stance when increased force is applied to the ground (Riegger, 1988). Independence between the metatarsal bones is necessary to allow all of the metatarsal heads to maintain contact with the ground in order to transmit force when the heel is raised (Hutton *et al.*, 1982) and to produce forefoot twist (Hicks, 1953). Independent movement of the metatarsals is not possible with the foot models by Inman and Mann (1978), nor its extended version by Morlock and Nigg (1991). These models assume that the forefoot is divided into only two segments: the first contains the navicular, three cuneiforms and the three medial metatarsals, and the second contains the cuboid and the two lateral metatarsals. The present model assumed that the first, third, fourth and fifth metatarsal bones have independent motion from the mid-tarsal segment, whereas the second was attached rigidly. The attachment of the second metatarsal to the mid-foot segment was necessary to allow kinematics of the transverse tarsal to be collected (see Methods), but was only plausible because of the restricted motion available between the three cuneiforms and the second metatarsal. Although, there are three anatomically defined tarsometatarsal joints, medial, intermediate and lateral (Moore, 1985), a separate tarsometatarsal joint was assumed to attach each metatarsal to the mid-tarsal segment (i.e. first tarsometatarsal joint for the first metatarsal bone).

The heads of each metatarsal bone are biconvex, whereas the proximal phalangeal bases of each toe are biconcave. This permits both plantar intraflexion and dorsiflexion, and abduction and adduction (Burns, 1987). We modelled only the plantar–dorsiflexion motion which is considerable during walking (Burns, 1987; Bojsen-Moller and Lamoreux, 1979; Hutton *et al.*, 1982). The model only considered the hallux because the four toes provide minimal load support during stance (Betts *et al.*, 1980; Hennig *et al.*, 1982).

The solution of the joint kinematics from kinesiological data required an estimate of the compression of the soft tissue on the plantar surface of the foot (see Methods). This soft tissue provides a cushion between the ground and the skeletal system. The structure of the heel pad has been analyzed in several classical studies (Blechschmidt, 1934; Kuhns, 1949; Tietze, 1921). Impact loads on the heel fat pad demonstrate that it has viscoelastic properties (Bennett and Ker, 1990; Cavanagh *et al.*, 1984; Ker *et al.*, 1987; Nakamura *et al.*, 1981; Thompson, 1988; Valiant, 1984). The heel pad was modelled as a nonlinear spring and a nonlinear damper, with the damper being dependent upon both strain, ε, and strain rate, $\dot{\varepsilon}$. The force, F_p, transferred by the tissue was defined by the equation

$$F_p = j\varepsilon^k + l\varepsilon^m|\dot{\varepsilon}|^n, \quad (1)$$

where j and k define the spring and l, m and n define the damper characteristics. The parameters were estimated using data from impact loads on the heel pad (Valiant, 1984). Discrete points at 1 ms intervals were measured from force–time and force–deformation plots from Valiant and converted to force, strain and strain rate assuming a heel pad thickness of 1.78 cm (Steinbach and Russell, 1964). The parameters of equation (1) were solved using an iterative, nonlinear, least-squares approach. The spring constants were defined from data during tissue compression. The damper constants were solved separately for compression and decompression of the tissue because of the complex architecture of the tissue (Table 1). Note the reverse in sign for parameter l since the absolute value of the strain rate is required mathematically. The large difference between parameter l for the compression and decompression of the soft tissue suggests the damper characteristics of the plantar fat pad is more predominant during compression. The model predicts force–deformation curves that are similar to the experimental results of Valiant (Fig. 2).

The soft tissue under the metatarsal bones and toes consists of subcutaneous fat, tendons, ligaments, the

Table 1. Values for the constants in equation (1) to define the soft-tissue model. j and k for decompression were set equal to compression values. Note the large difference in the value of l, the 'gain' of the damper (viscous) element, for compression and decompression

Constant	Compression	Decompression
j	1401	1401
k	3.46	3.46
l	2764	−48
m	4.84	4.30
n	0.99	0.33

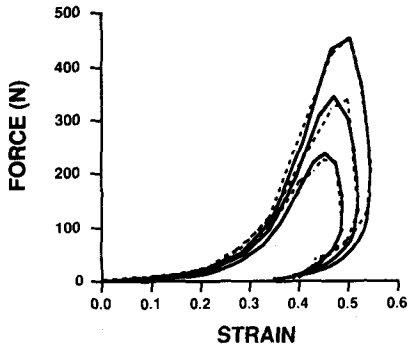

Fig. 2. The mechanical response of the human heel pad to impact loads at three different impact velocities from Valiant (1984) (solid line). The soft-tissue model (dashed line) effectively reproduced the force–time curves for the three impacts.

plantar aponeurosis insertion, and submetatarsal cushions (Bojsen-Moller and Flagstead, 1976). Changes in the mechanical properties of this tissue have been shown to occur during dorsiflexion of the metatarsophalangeal joints, which tightens the tissue under the heads of the metatarsal bones (Bojsen-Moller and Lamoreux, 1979). As well, the small distance between each metatarsal bone would reduce lateral dissipation within the tissue as seen at the heel pad (Valiant, 1984). However, there is no quantitative information on the force–deformation characteristics of the soft tissues under the metatarsal bones or toes. As a first approximation, the mechanical characteristics of the metatarsal and toe pads were assumed to mimic those of the heel pad. The force supported by the tissue per unit of deformation was assumed to be proportional to the area of contact under each segment; estimates used in the model are defined in Table 2. The average thickness of the soft tissue under the metatarsal bones was estimated using sagittal plane X-rays (Table 2).

Table 2. Estimates of the area of contact and soft-tissue thickness of each loading site. A large contact area supports a larger force for a given amount of strain compared to a small contact area

Location	Contact area (sq cm)	Thickness (cm)
Heel	19.6	1.8
First metatarsal	12.6	1.3
Second metatarsal	7.1	1.3
Third metatarsal	7.1	1.3
Fourth metatarsal	7.1	1.3
Fifth metatarsal	7.1	1.3
Hallux	7.1	0.5

METHODS

Several different reference frames were attached to the model to describe its motion, as well as a global reference system (G) that was fixed to the laboratory. The horizontal plane for the laboratory reference frame was defined by the x-axis, parallel with the plane of progression, and the z-axis, perpendicular to the plane of progression. The y-axis was directed upward and perpendicular to the floor. A local reference system (LRS) was attached to the calcaneus, LRS_c, and oriented initially with G. The transformation between G and LRS_c was defined by the matrix $[M]_{gc}$. All transformation matrices were defined by translation in the three orthogonal directions and successive rotations about the z-, y- and x-axis. LRSs were also attached to each joint and fixed to the proximal segment (Fig. 3). The z-axis for each joint LRS was aligned with the respective joint axis and the x-axis was aligned initially with the long axis of the distal segment. This orientation enabled rotations at each joint to be defined in its xy plane. A reference system was attached to the calcaneus at the transverse tarsal joint, LRS_2, and was defined relative to LRS_c by the transformation matrix, $[M]_{c2}$. The mid-tarsal segment was defined by the centroid of the second metatarsal head, $[P_2]$. The transformation of this point from G coordinates to LRS_2 coordinates, $[p_2]_2$, was defined by

$$[p_2]_2 = [M]_{c2}[M]_{gc}[P_2]. \quad (2)$$

Rotation of the transverse tarsal joint, α_{TT}, was defined by

$$\alpha_{TT} = \tan^{-1}\frac{y_2}{x_2}, \quad (3)$$

where x_2 and y_2 are coordinates from $[p_2]_2$.

Reference systems were attached to the tarsal segment at each of the tarsometatarsal joints, LRS_i, where $i = 1, 3, 4, 5$. Each LRS was defined relative to LRS_2 by the transformation matrix, $[M]_{2i}$. The transformation of the centroid of each metatarsal head from G coordinates, $[P_i]$, into its corresponding tarsometatarsal coordinates, $[p_i]_i$, were defined by

$$[p_i]_i = [M]_{2i}[M]_{c2}[M]_{gc}[P_i],$$

where $i = 1, 3, 4, 5.$ (4)

Rotation of each tarsometatarsal joint, α_{iT}, was defined by equation (3) using the local metatarsal coordinates, x_i and y_i from $[p_i]_i$.

A reference system was attached to the first metatarsal segment at the first metatarsophalangeal joint, LRS_6, and was defined relative to LRS_1 by the transformation matrix, $[M]_{16}$. The transformation of the point on the midline of the hallux from G coordinates, $[P_6]$ to the first metatarsophalangeal coordinates, $[p_6]_6$, was defined by

$$[p_6]_6 = [M]_{16}[M]_{21}[M]_{c2}[M]_{gc}[P_6]. \quad (5)$$

Rotation of the first metatarsophalangeal joint, α_{MP}, was defined by equation (3) using the hallux coordinates, x_6 and y_6 from $[p_6]_6$.

The kinematics and kinetics of the foot were estimated during normal walking for three subjects (Table 3; also used in Scott and Winter, 1991). To begin, the

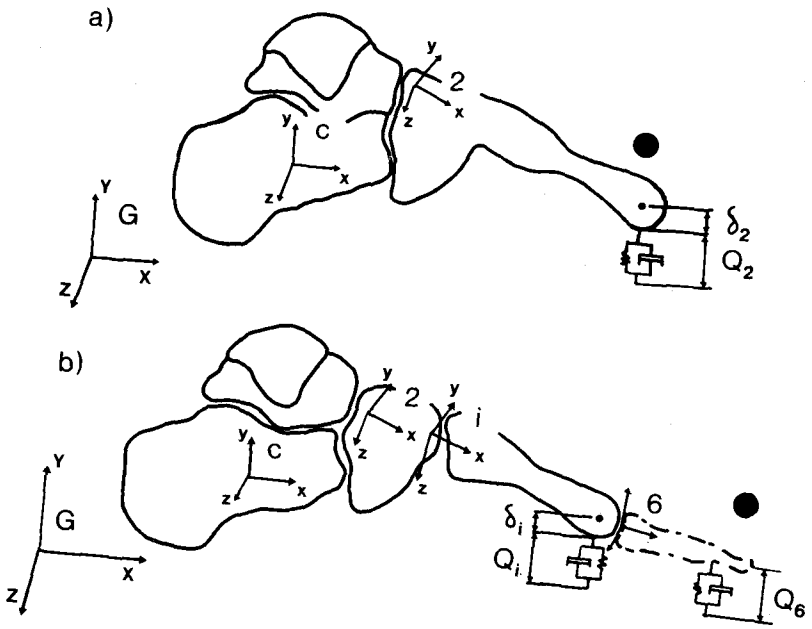

Fig. 3. A global reference frame (G) was attached to the laboratory and local reference frames were attached to the calcaneus (c) and at each joint (2, *i*, 6). Each joint reference frame was always attached to the proximal segment. (a) Lateral view: the vertical position of the mid-tarsal segment was described by the position of the second metatarsal head. This was defined by estimating its position above the ground based on its radius, δ_2, and the thickness of the underlying soft tissue, Q_2. The three-dimensional position of the second metatarsal was also defined using a surface marker attached to the overlying skin (black circle). (b) Lateral view: the position of each metatarsal, *i*, was defined like the mid-tarsal segment. The vertical position of the hallux was defined by the soft-tissue compression, Q_6. Its three-dimensional position was also defined by a surface marker attached to the toe nail (black circle).

Table 3. Subject anthropometric data. The dimensions of the foot were used to scale the position of the transverse tarsal and the tarsometatarsal joints for each subject

Subject	WK04	WK22	WK23
Sex	F	M	M
Age	22	22	29
Height (cm)	168	180	173
Weight (kg)	52.4	72.8	65.1
Foot length (cm)	24.8	25.6	26.0
Foot width* (cm)	8.2	10.2	9.0
Foot height† (cm)	6.8	7.7	7.8

*Across the metatarsa; heads
†Above the navicular

position of each joint and contact point under the foot had to be defined for each subject. The position and orientation of the transverse tarsal joint axis was defined initially by the position of the talonavicular and the calcaneocuboid joints from Salathé *et al.* (1986). The position of each tarsometatarsal joint was aligned in the transverse plane perpendicular to the longitudinal axis of its respective metatarsal bone, based on the coordinates from Salathé *et al.* (1986). The location of these joints were scaled to each subject in the three orthogonal directions, *x*, *y*, and *z*, based on their foot length, height above the navicular bone, and width at the heads of the metatarsal bones, respectively. The position of the head of each metatarsal was located by palpation on the sole of the foot on each subject and marked relative to a chalkprint of the foot. This chalkprint acted as a template to allow the position of each metatarsal and the hallux to be defined on chalkprints which were taken during contact with the force plate during the walking trials (see below). The first metatarsophalangeal joint axis of rotation was located at the head of the first metatarsal. The midline of the hallux was defined by the bisection of the widest portion of its plantar chalkprint.

The position of the foot segments during walking were estimated using two different techniques. The calcaneus was located in three-dimensional space using surface markers. The data collection procedures for surface markers and force-plate measurements during these walking trials have been described previously (Scott and Winter, 1991). The positions of the other segments were described by estimating the position of a single point on each segment. These points of interest of each segment were (1) the centroid of the second metatarsal head for the mid-tarsal segment, (2) the centroid of the other metatarsal heads for each of their respective segments, and (3) the bisection of the widest portion of the plantar chalkprint of the hallux for the hallux segment. Surface markers could not be used to determine the position of all these distal

segments using our data collection system. Instead, we estimated the position of these segments from the position and loading of the soft tissue under each segment. To begin, we describe how the horizontal position of the point of interest on each segment was determined. This is followed by an explanation of how we estimated the vertical position of the single point on each segment based on the compression of the soft tissue.

Foot placement on the force plate was determined by covering the bottom of the foot with blue carpenter's chalk and recording the footprint on non-glossy, textured paper that covered the force plate (Munro *et al.*, 1987). These prints were compared to footprints where the metatarsal heads and hallux had been defined (see above) and allowed the X and Z coordinates of the point of interest on each of the segments to be calculated.

When the heel rises during walking, the metatarsal bones rotate with the heel and their contact with the ground is shifted forward. This was corrected by estimating a new coordinate, X_i', for each metatarsal segment based on,

$$X_i' = X_i + \frac{2\pi\delta_i}{\alpha_c}, \quad \text{where } i = 1, \ldots, 5, \qquad (6)$$

where α_c was the sagittal plane rotation of the calcaneus in radians and δ_i is the radius of curvature of each metatarsal head as defined by the averaged values from Stokes *et al.* (1979). This forward shift of the contact point was not considered for the hallux.

The vertical position, Y_i, of each metatarsal head and the hallux was estimated by adding its radius with the thickness of the plantar soft tissue. The thickness of the plantar tissue required a measure of its compression during the stance phase using equation (1), which required an estimate of the load supported by each individual foot segment. Therefore, an extra set of walking trials measured the ground reaction force (GRF) on a modified force platform. A small force plate (approximately 11 cm^2) was made that attached onto the original AMTI force platform providing a smaller active region. The accuracy of this small plate was tested and found to be similar to the original large platform. A walkway was used to provide a walking surface flush with the small plate. The force plate was recalibrated for measurement of both the GRF and the center of pressure (CP) on the small plate. Force-plate trials were collected digitally at 400 Hz and filtered using a zero-lag, fourth-order Butterworth filter with a 30 Hz cut-off frequency (Winter, 1990; Winter *et al.*, 1974). The GRF and CP data were then resampled at 60 Hz and stored for analysis. Foot placement on the force plate was again determined from chalk footprints.

The subjects were instructed to walk across the force plate while looking forward. The subjects walked at their selected cadence and their starting position was set to allow foot contact with the plate. The fixed distance from their starting position to the plate controlled the stride length, thus helping to maintain a constant walking cadence and speed throughout all trials (Lamoreux, 1971).

Heel and hallux loads could be collected separately when either site contacted the force platform, while the remainder of the foot landed in front or behind the plate, respectively. Heel loads were recorded for further analysis if the heel landed on the plate and a 5 cm region halfway between the metatarsals and heel contacted the edge of the plate. Hallux loads were selected if the hallux landed on the plate and the gap between the distal phalanx of the hallux and the soft-tissue pad of the first metatarsal bone landed on the edge of the plate, as defined by the chalkprint. The load under the other toes contributed to the measured hallux force, but the magnitude sustained by these structures is known to be relatively small (Betts *et al.*, 1980; Hennig *et al.*, 1982). The location of the spring and damper representing the soft tissue under each segment required that a single point be selected under the hallux, $[P_6]$, and the heel, $[P_c]$. These coordinates were estimated by multiplying the CP recorded for the individual segment by its corresponding vertical GRF, summing these products for all of the stance phase, and then dividing by the sum of the vertical GRF for all of the stance phase.

The load sustained by each metatarsal bone was assumed to be centered directly below the centroid of its head. Force-plate trials could measure the load acting under a single metatarsal only rarely and then only for the first and fifth metatarsal. Instead, trials were collected in which one or more metatarsal heads contacted the force platform. Decomposition of the force sustained at each metatarsal head was estimated using the magnitude of the GRF and its CP coordinates (see Appendix). Several repeat trials were also recorded for (1) the complete foot, (2) the metatarsus and toes only, and (3) the heel and metatarsus only. These trials allowed the timing of loads at each loading site to be defined relative to total stance time.

The load distribution of the GRF assumed that the force was distributed at seven identifiable regions and that each region could be represented as a single loading site. The suitability of these assumptions was tested by comparing the GRF and CP for the entire foot with the estimated curves created by the summation of the estimated loads acting at each loading site. Eight complete-foot force-plate landings were performed by each subject and the GRF and CP trajectory averaged. These were compared to the vertical GRF, GRF^{pred}, and the CP coordinates, $[CP]^{pred}$, determined by

$$GRF^{pred} = \sum GRF_i, \qquad (7)$$

$$[CP]^{pred} = \frac{\sum([P_i]GRF_i)}{GRF^{pred}}, \qquad (8)$$

where GRF_i is the estimated vertical GRF at each loading site and $[P_i]$ is its coordinates.

The GRF acting under each region of the foot was scaled for the walking trials where joint kinematics and kinetics were estimated. First, the force acting under each loading site, GRF_i, was divided by GRF^{pred} for each increment in time. The time base for stance was shortened or lengthened for these individual loads to correspond to the actual stance time for the walking trial using linear interpolation. These fractions were then multiplied by the GRF recorded during the kinematic and kinetic walking trials. This scaling approach meant that total stance time and the load supported by the foot was correct for each walking trial. Only the distribution of the load under the foot was fixed for all trials. For purposes of calculating the joint moments, it was assumed that the distribution of the shear forces under the foot was proportional to the vertical force. For example, if a loading site sustained 20% of the total vertical GRF at a specific time during the stance phase, then it was assumed that it also sustained 20% of the total shear force at that time.

The second procedure necessary to determine the thickness of the soft tissue was an estimate of its compression based on the soft-tissue model. An iterative solution of soft-tissue strain, ε_i, at each loading site was performed using equation (1), where F_p equalled GRF_i. Y_i, the vertical coordinate of $[P_i]$, was defined by adding the thickness of the soft tissue, Q_i, with the radius of the metatarsal head, δ_i. This equalled

$$Y_i = Q_i(1-\varepsilon_i)+\delta_i, \quad \text{where } i=1, \ldots, 6. \tag{9}$$

Initially, the magnitude of the fat-pad strain was predicted to oscillate during flatfoot due to the residual noise in the marker data. Motion of a fraction of a millimetre between frames created large strain-rate estimates resulting in nonphysiological deformation patterns. Therefore, the damper component of the fat-pad model was implemented only during initial compression of the tissue.

The coordinate data used in this model were obtained from three different techniques: markers on the calcaneus digitized using a video analysis system, chalk footprints to define the X and Z coordinates of the 6 distal segments and a soft tissue model to estimate the Y coordinate of these segments. Slight discrepancies (± 5 mm) between coordinates from the different data-collection techniques resulted in slight shifts (approx. 3°) in the estimated joint rotations between trials. Therefore, joint rotations were averaged based on the mean of the signal for each trial. Neutral joint position was defined by initial contact of the distal segment with the ground.

Many assumptions were required to estimate the joint kinematics from footprints and the soft-tissue compression. These results were compared to joint rotations predicted using spherical markers on two of the distal segments: the second metatarsal and the hallux. The position of each marker was digitized by the video analysis system and used to estimate the transverse tarsal and metatarsophalangeal joint rotation, respectively. Neutral joint position was also defined by initial contact of the distal segment with the ground.

Gravitational and inertial forces were not included in the joint moment estimates because their magnitudes are small during the stance phase of walking (Winter, 1990). The joint moment of force, $[T_i]_i$, was defined by the vector product

$$[T_i]_i = [p_i]_i \times [\text{grf}_i]_i, \quad \text{where } i=2, 3, 4, 5, 6, \tag{10}$$

where $[p_i]_i$ and $[\text{grf}_i]_i$ are the loading site and force vector, respectively, transformed into the corresponding joint LRS. The z component of each joint LRS was aligned with the joint axis of rotation. Therefore, the z component of $[T_i]_i$ represents the moment of force acting about the joint axis. Equation (10) was used to calculate the joint moments at the third, fourth and fifth tarsometatarsal and the first metatarsophalangeal joints. The joint moment at the second tarsometatarsal joint was also calculated using equation (10) for comparison to the other joint moments. The other two joints had more than one loading site acting upon them. The GRF acting upon the transverse tarsal joint, $[GRF_2]$, was determined by

$$[GRF_2] = [GRF_t]-[GRF_c], \tag{11}$$

where subscript t and c denote total and heel GRF, respectively. The center of pressure, $[CP_2]$, was determined using

$$[CP_2] = \frac{[CP_t][GRF_t]-[CP_c][GRF_c]}{[GRF_2]}. \tag{12}$$

The transverse tarsal joint moment, $[T_2]$, was defined by equation (10), where $[cp_2]_2$ was substituted for $[p_i]_i$.

The first tarsometatarsal joint moment includes the effects from the GRF acting at the first metatarsal head, as well as the force under the hallux. The joint moment, $[T_1]_1$, was determined by

$$[T_1]_1 = [p_6]_1 \times [{}^3\hat{O}\hat{C}\hat{O}\hat{M}e_3]_1 + [p_1]_1 \times [\text{grf}_1]_1 \tag{13}$$

RESULTS

Many repeat trials were required to estimate the GRF acting under each loading site (average collected = 129, average analyzed = 40). Further analysis of the data and the footprints eliminated some trials and reduced the number of trials used to decompose the load under each region of the foot. Contact times for each region of the foot were slightly different between subjects, but were within the expected range (Soames, 1985).

The force under each metatarsal head increased gradually during stance phase and peaked between 75 to 90% of stance phase. Subject WK23 had a similar distribution of load between the second, third, fourth and fifth metatarsals, but the first sustained only a very small force (Fig. 4). The trial-to-trial variability of the

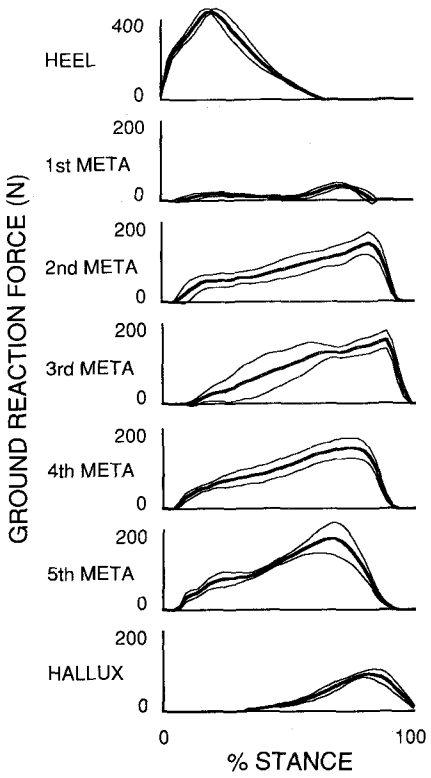

Fig. 4. The estimated ground reaction force (GRF) acting at each loading site for subject WK23. The thick line denotes the mean values, while the thin lines denote 1 standard deviation. Note the similarity between the GRF acting under each metatarsal and the corresponding tarsometatarsal joint moment in Fig. 8.

force sustained at each loading site for subject WK23 was similar to the variability seen for the other two subjects. Subject WK04 generated large peak loads under the second and third metatarsals and small loads acting on the other three metatarsals (Table 4). Subject WK22 had large loads under the second, third and fifth metatarsals. This subject's fifth metatarsal bone consistently supported a very large force reaching 220 N during mid-stance, contrasting with most other metatarsal-load estimates that peaked late in the stance phase. The temporal pattern of loading at each of the forefoot contact sites are quite similar to the temporal pattern of the tarsometatarsal joint moments (compare Fig. 4 to WK23 in Fig. 8).

The force acting under the hallux began to build gradually during flatfoot and slowly increased to a peak at a time between 80 and 85% of the stance phase (Fig. 4). Peak loads ranged from 95 N for subject WK23 to 260 N for subject WK22. This latter subject was walking noticeably faster than the other two, although no exact measure of walking velocity was recorded.

The estimated GRF and CP pathway estimated from the summation of force at each loading site were similar to the results obtained from whole-foot force-plate trials. The comparison between estimated and measured GRF and CP illustrated in Fig. 5 is typical

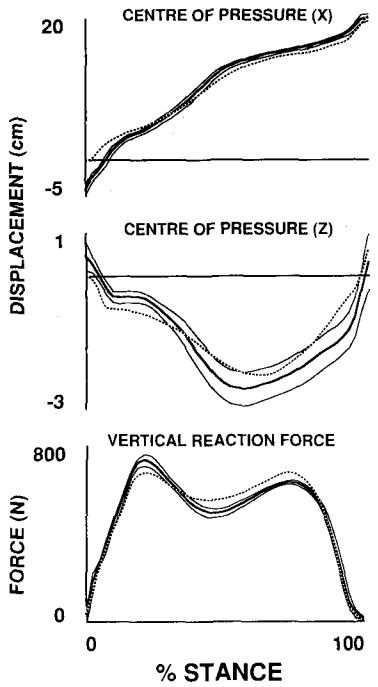

Fig. 5. The ground reaction force (GRF) and its center of pressure (CP) during the stance phase of walking for subject WK23. The thick line denotes mean, while the thin lines denote 1 standard deviation. Similar GRF and CP profiles were produced by summing the estimated loads acting at the seven loading sites (dotted lines) and substantiates the use of seven separate points of contact between the foot and ground in the model.

Table 4. The peak forces and their standard deviation acting at each of the seven loading sites under the foot. The number of trials used to estimate the force at each particular site is given in brackets. Note the difference in loads under each metatarsal within and across subjects

Loading site	Segment no.	WK04	WK22	WK23
Heel	0	476±26 (4)	635±30 (5)	446±9 (5)
First metatarsal	1	73±8 (4)	101±28 (5)	37±6 (4)
Second metatarsal	2	170±39 (7)	158±15 (4)	147±28 (4)
Third metatarsal	3	141±24 (7)	164±54 (4)	160±22 (5)
Fourth metarsal	4	75±40 (6)	106±33 (3)	153±26 (3)
Fifth metarsal	5	37±7 (2)	220±23 (4)	180±38 (6)
Hallux	6	150±13 (6)	260±62 (4)	94±10 (4)

for all subjects. At heel contact, the estimated X component of the CP trajectory (dotted) was fixed at the origin, while the actual CP trajectory (thick solid) was negative. The model assumed that the CP equalled the heel load coordinate, $[P_0]$, while the true contact between the heel and ground was slightly posterior of the heel coordinate because the forefoot was elevated. The peak negative excursion of the CP in the Z direction was underestimated by the model for subject WK04, but the magnitude of this error was under 7 mm. Such a discrepancy could have been caused by an overestimation of the force at loading sites on the medial side of the foot and/or by an underestimation of the loads at sites on the lateral side.

Joint rotations could only be estimated when the distal segment was in contact with the ground. Positive rotation was defined as extension of the joint, the distal segment was deflected dorsally. The magnitude of joint rotations shows a wide range of variability between joints and between subjects (Fig. 6). In one subject, the transverse tarsal joint extended slightly during mid-stance (WK04 in Fig. 6). The other two subjects did not demonstrate any rotation at this time. During push-off, the three subjects flexed these joints 5–10° just before the second metatarsal head left the ground. For subjects WK04 and WK22, this joint flexion goes below neutral joint orientation.

An understanding of the significance of the tarsometatarsal joint rotations requires a comparison of the angle of each joint at flatfoot (40% of stance) and during push-off (90% of stance). At flatfoot, all the metatarsals contact the ground and the transverse tarsal and tarsometatarsal joints show minimal rotation. At push-off, the heel is well above the ground and the lateral tarsometatarsal joints rotate and maintain contact with the ground. A decrease in the magnitude of the flexion is evident from the fifth to third tarsometatarsal joints. Flexion of the fifth tarsometatarsal joint ranged from 4 to 12° compared to −1 to 2° of flexion for the third tarsometatarsal joint. Flexion of the first tarsometatarsal at 90% stance for subjects WK04 and WK22 were 2 and 6°, respectively.

Similar rotations at the transverse tarsal joint were found if the model assumed that the soft tissue was incompressible under the head of the second metatarsal bone (Fig. 7). Small changes were evident at the beginning and end of contact by the second metatarsal bone with the ground. Similar rotations were also seen when the position of the mid-tarsal segment was defined by a surface marker (Fig. 7). As well, the surface marker estimated about 5° of flexion before the metatarsal bone touched the ground and at toe-off, a further 5–10° of flexion was estimated for subjects WK22 and WK23. In total, the transverse tarsal joint

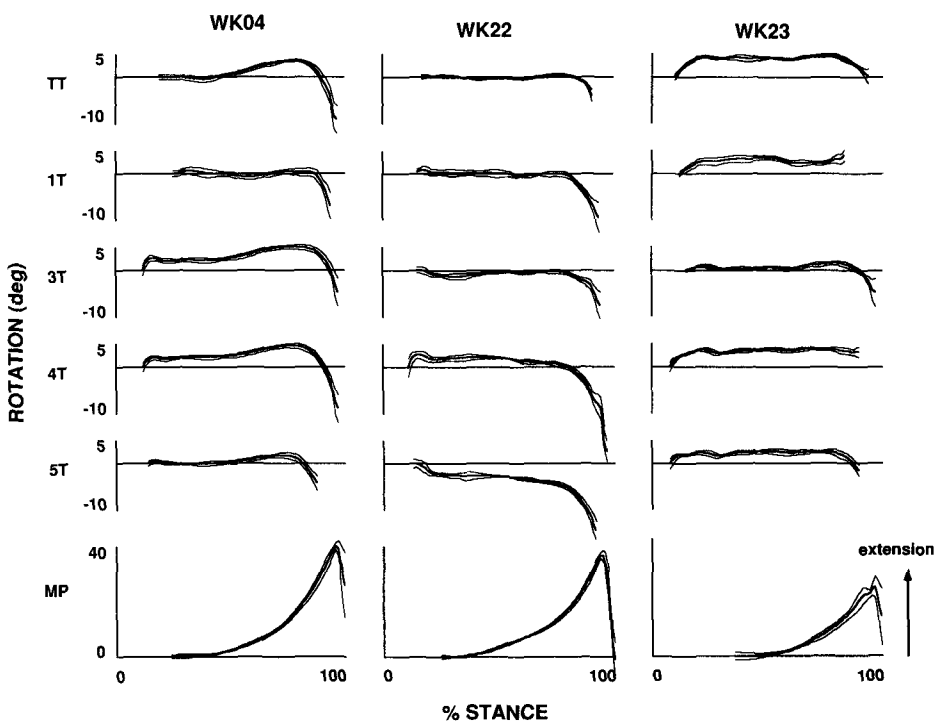

Fig. 6. The joint rotations estimated for each subject. The thick line denotes mean, while the thin lines denote 1 standard deviation. The transverse tarsal and the tarsometatarsal joints show a variable amount of extension during mid-stance followed by rapid flexion during the end of stance. Note that the fifth tarsometatarsal joint is the first joint to rotate negatively during late stance in order that the head of the fifth metatarsal may remain in contact with the ground. The metatarsophalangeal joint extends significantly at this time. Joint acronyms are defined in Fig. 1.

was estimated to flex between 10 and 20° during push-off for these three subjects.

The first metatarsophalangeal joint extends positively from the end of flatfoot to approximately 95% of stance (Fig. 6). The joint rapidly flexes during the last 5% of stance. However, the surface marker estimated somewhat larger joint extension for both subjects WK22 and WK23 (Fig. 7). The magnitude of joint flexion at the end of stance was also estimated to be much smaller when the position of the segment was defined by the marker rather than from chalkprints and soft tissue compression.

The peak flexor moment of force estimated at the transverse tarsal joint ranged from 54 to 83 Nm and occurred just before 80% stance (Fig. 8). This represents about two thirds of the peak moment estimated

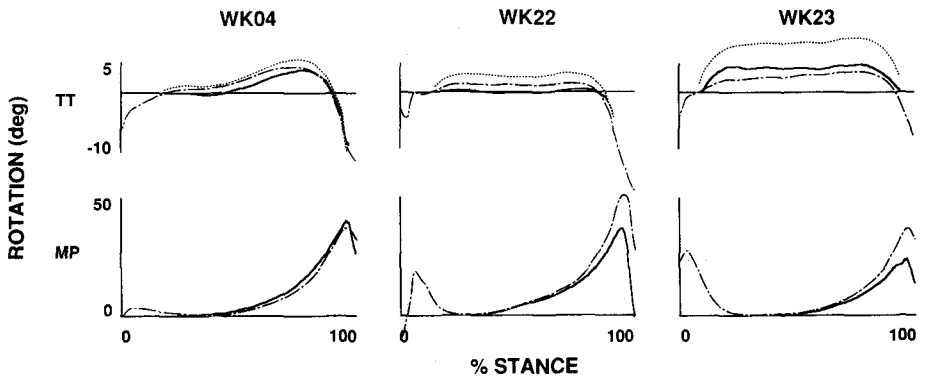

Fig. 7. The estimated rotation at the transverse tarsal joint (TT) was similar whether it was based on a compressible soft tissue model (solid; same as Fig. 6), or an incompressible soft-tissue model (dashed). Therefore, joint rotation measurements were not very sensitive to the properties of the soft tissue model. Similar rotation at the TT joint was also estimated by a surface marker above the second metatarsal (dot-dashed) suggesting that the position of the second metatarsal could be estimated adequately using chalk footprints and the soft-tissue model. The estimated rotation of the metatarsophalangeal joint (MP) was not always similar when the segment position was defined by a surface marker (dot-dashed) and when it was defined using the soft-tissue model (solid; same as Fig. 6). The estimate based on the soft tissue model was probably inaccurate because the loading site under the hallux was not assumed to move forward when the hallux rotated during toe-off.

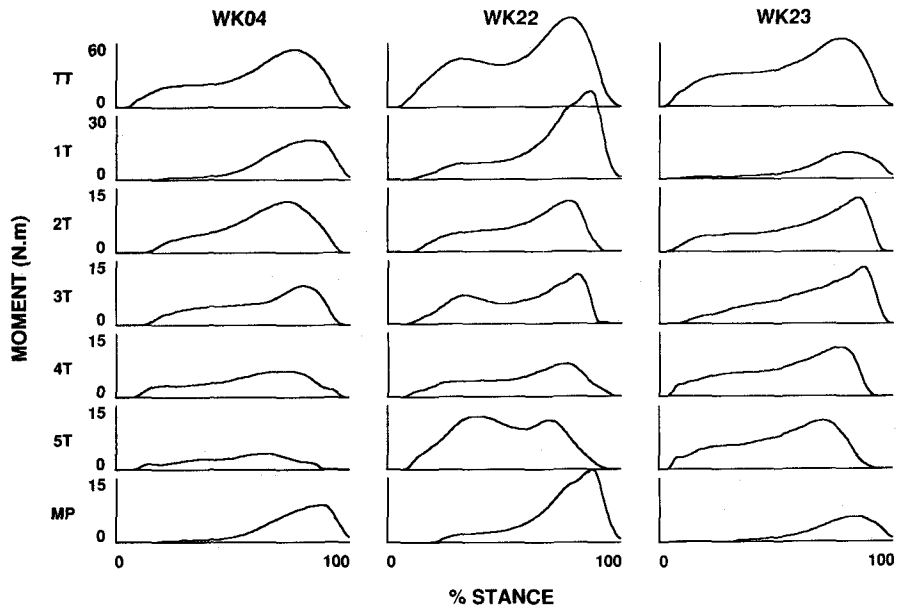

Fig. 8. The estimated moments of force at each joint during the stance phase of walking. The large differences in the joint moments for different subjects were largely due to the variability in the distribution of the GRF under the foot. 2T is the second tarsometatarsal joint; other joint acronyms are defined in Fig. 1.

to occur at the talocrural joint, but more than double the magnitude of the peak moment at the talocalcaneal joint (Scott and Winter, 1991).

The moments acting at the tarsometatarsal joints show a consistent pattern of loading that was highly dependent on the GRF estimate. This is evident by comparing the GRF in Fig. 4 at the second, third, fourth and fifth metatarsals and the hallux with the joint moments of force in Fig. 8 for the second, third, fourth and fifth tarsometatarsal and the metatarsophalangeal joints, respectively. The standard deviation between trials is not shown because their variability was artificially low; this was a consequence of the fixed distribution of the GRF between loading sites (see Methods). Peak moments ranged from 4 to 15 Nm for the second to fifth tarsometatarsal joints during walking. Much larger values were evident at the first tarsometatarsal joint because of the GRF acting on the hallux. The large moment estimated for WK22 was created by a 260 N force acting under the toes, compared to forces of 150 N or less under the toes by the other subjects. These moments were slightly high because the load attributed to the hallux included the small load sustained by the lateral toes.

The first metatarsophalangeal joint moment was small during flatfoot, but increased rapidly to a peak at about 90% of stance. The estimated moment reflects the metatarsophalangeal joint moment acting about all of the metatarsophalangeal joints because of the inclusion of the GRF for all the toes in the load estimate for the hallux.

DISCUSSION

The complexity of the foot and its contribution to locomotion is vastly underrated. The foot provides a compliant, yet sufficiently rigid interface to transmit propulsive forces from the body to the ground. The purpose of this study was to develop a three-dimensional model of the foot that could be used to describe foot mechanics during walking. The results demonstrate measurable movement within the foot that can be described using the model. Arguably, the present model is too complex for most direct dynamical human models or for many specific questions regarding foot function. However, the salient features of the present model and results should be incorporated in future dynamic human models if they are to be effective in simulating human locomotion.

Several novel techniques were developed in this study in order to calculate the kinematics and kinetics of the foot. The position of the segments distal to the calcaneus were obtained using two different techniques; their horizontal positions were measured from footprints, whereas their vertical positions were based upon a model of the plantar soft tissue. Rotations at the transverse tarsal joint were similar whether the soft tissue was assumed to be compressible or incompressible, or whether the position of the segment was estimated from a surface marker (Fig. 7). However, there was some differences in the metatarsophalangeal joint rotations estimated by the different techniques. In this case the surface marker would probably be more reliable since it was attached rigidly to the toe nail. Movement of the contact site due to rotation of the hallux during toe-off was not considered in the soft-tissue model. A correction for segment rotation was used to move the contact site under the metatarsal bones [equation (6)] and minimal differences were found between the two techniques. The use of surface markers had the added advantage that segment position could be estimated whether or not the segment was in contact with the ground. It might be advantageous to use a positional data-collection system to analyze movements of all the distal segments, but only if the system could resolve the position of each of the closely spaced markers on each metatarsal and if the position of these markers were not susceptible to skin–bone motion. For example, markers on the fifth metatarsals may be susceptible to movement from compression of the underlying soft tissue, whereas the first metatarsal may be susceptible to movement by the tendon of extensor hallucis longus.

The model required an estimate of the load sustained at seven separate sites under the foot. The force plate, traditionally used to measure the GRF under the foot, could not be used for this purpose because it can give only the total force and its CP under the foot. A measure of the GRF acting at each loading site can be estimated by individual transducers that measure the pressure at discrete locations (Gross and Bunch, 1988; Soames, 1985). However, these transducers may give inaccurate results if they are not positioned precisely at each loading site because large pressure gradients are created under the foot during stance (Hennig *et al.*, 1982). Two attractive methods to determine the distribution of load beneath the foot during walking involve either glass-plate illumination (Betts *et al.*, 1980; Duckworth *et al.*, 1982) or the use of a matrix of pressure transducers (Hennig *et al.*, 1982). Each gives a complete picture of pressure under the entire surface of the foot, but their cost was prohibitive for purposes of this study. Therefore, estimates of the loads were decomposed from walking trials where only part of the foot landed on a small force platform (see Methods). The summation of the contact loads under the foot reproduced the true GRF and CP data from force-plate trials where the whole foot contacted the force plate (Fig. 5). There was a large variability in the load for a given contact site between subjects, but the variability was similar to the variability in the results of other foot studies (Betts *et al.*, 1980; Duckworth *et al.*,1982; Hennig *et al.*, 1982; Stott *et al.*, 1973).

However, our rather arduous method to estimate the load at different sites under the foot had several drawbacks. First, it was tedious to perform and analyze the many trials. Second, errors in the estimates of joint rotations may have been caused by differences in the onset and offset of contact at individual loading

sites for walking trials used to estimate the load distribution under the foot as compared to walking trials in which the kinematic data was collected. Finally, the use of averaged loads under the foot constrained the center-of-pressure path. Therefore, the actual trial-to-trial variability in the center-of-pressure path did not influence the variability in the joint moment profiles. An improved measure of the moment-of-force variability would have been possible if the load distribution under the foot was estimated using a matrix of force transducers (Hennig *et al.*, 1982), while the kinematic data were being collected.

There are many assumptions required to develop the present model of the foot and it is important to understand how these assumptions might affect the model results. The soft-tissue spring and damper model was based on force–deformation data from Valiant (1984). More recent studies suggest that the heel pad is much more resilient (Bennett and Ker, 1990; Ker *et al.*, 1987). However, joint kinematics were only affected marginally from the soft-tissue characteristics and only at initial contact (Fig. 7). The kinematics were also similar if a surface marker was used to define the position of the mid-tarsal segment suggesting that the soft-tissue model does not alter the estimated joint kinematics significantly.

The most contentious assumptions in the model pertain to the fact that motion was constrained to occur at only a few of the anatomically defined joints that were expected to provide the greatest range of motion and that these joints were considered to be monocentric with a single degree of freedom. It would be naive to think that the foot actually works in such a simplified fashion; motion will occur at many of the joints spanning the metatarsals and the calcaneus and the rotation of these joints will not necessarily be restricted to a single degree of freedom nor a single axis of rotation. As described previously, the selection of the joints within the model were defined from information from the literature (see the Model). A recent study by Ouzounian and Shereff (1989) quantified motion at each of the articulations of the mid-foot. Although the loading conditions for their study were generally lower than those during walking, their study provides a useful comparison to our results. Their study suggested that the range of motion at the tarsometatarsal joints was greatest at the cuboid-fourth metatarsal (mean, 9.6°; S.D., ±4.97) and the cuboid-fifth metatarsal (mean, 10.2°; S.D., ±8.73). Our data suggest that the full range of motion at these joints is utilized during walking. Their study also suggested that the navicular–cuneiform joints provide measurable movement. This contradicts the present model which assumes these joints are locked. Fortunately, the model is not highly sensitive to motion at the navicular–cuneiform joint. If 10° of movement, attributed to occur at the transverse tarsal joint, actually occurred through equal motion at the transverse tarsal and the navicular–middle cuneiform, the total angular motion at both of these joints would increase by only 1° (each joint would rotate 5.5°). This assumes that the distance from the second metatarsal head to the navicular–middle cuneiform joint is 5 times the distance from the navicular–middle cuneiform joint and the transverse tarsal joint. In a similar manner, if 10° of motion attributed to occur at the first tarsometatarsal joint actually occurred through equal movement at both the tarsometatarsal and the navicular–medial cuneiform joint, the total movement at both joints would only decrease by about 1° (each joint would rotate 4.5°). The insensitivity of the joint rotations to movement at the navicular–cuneiform joints is largely due to the small size of the mid-foot bones relative to the long metatarsal bones. Although, our model cannot substantiate whether motion occurred at only one mid-tarsal joint, the model does provide a good measure of the total motion across all spanned joints.

The quantitative results of our study substantiate the qualitative description of foot function during locomotion. The transverse tarsal and the tarsometatarsal joints both flex and increase the height of the longitudinal arch at the same time that the metatarsophalangeal joint extends during push-off (Figs 6 and 7; Burns, 1987; Hutton *et al.*, 1982; Klenerman, 1982). It has been suggested that extension of the hallux and toes causes the plantar aponeurosis to be wrapped around the metatarsal heads, like a windlass, to pull the calcaneus towards the metatarsals (Hicks, 1954; Mann and Hagy, 1979). Kayano (1986) estimated that the longitudinal arch rises 6 mm during push-off which corresponds to approximately 10° of angular movement in the arch. This angular motion in the longitudinal arch compares favorably with the magnitude of the transverse tarsal movement for the three subjects in this study. The model estimates that the lateral tarsometatarsal joints rotate more than the medial tarsometatarsal joints during the push-off phase of stance (Fig. 6). The lateral metatarsals do not extend as far forward as the medial metatarsals. As a result, the lateral tarsometatarsals must rotate when the heel rises in order for the heads of the metatarsals to remain in contact with the ground. This flexion of the lateral tarsometatarsal joints during push-off is consistent with previous descriptions of metatarsal movement by Hutton *et al.* (1982).

In conclusion, the calculation of both the movements and loading within the foot provide important information on how the foot adapts to support the body during locomotion. The strong relationship between the results estimated with the foot model and previous qualitative descriptions of foot function suggest that the model may prove useful as an objective measure to understand foot function during normal and pathological movements. If three-dimensional models of the complete human body are used to simulate human locomotion, than the representation of the foot should include both viscoelastic plantar tissue, as well as an internal structure that allows the foot to adjust to the underlying substrate.

Acknowledgments—The authors would like to thank Drs G. E. Loeb, F. J. R. Richmond and W. S. Selbie for their valuable comments on the manuscript. The financial support of the Medical Research Council of Canada (Grant MT 4343) is acknowledged.

REFERENCES

Beckett, R. and Chang, K. (1968) An evaluation of the kinematics of gait by minimum energy. *J. Biomechanics* **1,** 47–159.

Bennett, M. B. and Ker, R. F. (1990) The mechanical properties of the human subcalcaneal fat pad in compression. *J. Anat.* **171,** 131–138.

Betts, R. P., Franks, C. I., Duckworth, T. and Burke, J. (1980) Static and dynamic foot-pressure measurements in clinical orthopaedics. *Med. Biol. Engng. Comput.* **18,** 674–684.

Blechschmidt, E. (1934) Die architektur des fersenpolsters. *Gegenbaurs Morphologisches Jahrbuch* **73,** 20–68 (reprinted as: The structure of the calcaneal padding. *Foot Ankle* **2,** 260–283, 1982).

Bojsen-Moller, F. and Flagstead, K. E. (1976) Plantar aponeurosis and internal architecture of the ball of the foot. *J. Anat.* **121,** 599–611.

Bojsen-Moller, F. and Lamoreux, L. (1979) Significance of free dorsiflexion of the toes in walking. *Acta Orthop. Scand.* **50,** 471–479.

Burns, M. J. (1987) Biomechanics. In *Fundamentals of Foot Surgery* (Edited by McGlamry, E. D.), Chap. 2, pp. 111–135. Williams & Wilkins, Baltimore, MD.

Cavanagh, P. R., Valiant, G. A. and Misevich, K. W. (1984) Biological aspects of modeling shoe/foot interaction during running. In *Sport Shoes and Playing Surfaces* (Edited by Frederick, E. C.), pp. 24–46. Human Kinetics Publishers, Champaign.

Chen, B.-R., Hines, M. J. and Hemami, H. (1986) Dynamic modelling for implementation of a right turn in bipedal walking. *J. Biomechanics* **19,** 195–206.

Chow, C. K. and Jacobson, D. H. (1971) Studies of human locomotion via optimal programming. *Math. Biosci.* **10,** 239–306.

Duckworth, T., Betts, R. P., Franks, C. I. and Burke, J. (1982) The measurement of pressures under the foot. *Foot Ankle* **3,** 130–141.

Elftman, H. (1960) The transverse tarsal joint and its control. *Clin. Orthop.* **16,** 41–45.

Engsberg, J. R. (1987) A biomechanical analysis of the talocalcaneal joint *in vitro*. *J. Biomechanics* **20,** 429–442.

Gross, T. S. and Bunch, R. P. (1988) Measurement of discrete vertical in-shoe stress with piezoelectric transducers. *J. biomed. Engng.* **10,** 261–265.

Hamilton, J. J. and Ziemer, L. K. (1981) Functional anatomy of the human ankle and foot. In *Proceedings of the AAOS Symposium on The Foot and Ankle* (Edited by Kiene, R. H. and Johnson, K. A.), p. 1–14. The CV Mosby Company, St. Louis.

Hennig, E. M., Cavanagh, P. R., Albert, H. T. and Macmillan, N. H. (1982) A piezoelectric method of measuring the vertical contact stress beneath the human foot. *J. biomed. Engng.* **4,** 213–222.

Hicks, J. H. (1953) The mechanics of the foot I. The joints. *J. Anat.* **87,** 345–357.

Hicks, J. H. (1954) The mechanics of the foot II. The plantar aponeurosis and the arch. *J. Anat.* **88,** 25–31.

Hutton, W. C., Stott, J. R. R. and Stokes, I. A. F. (1982) The mechanics of the foot. In *The Foot and Its Disorders* (Edited by Klenerman, L.) Chap. 3, pp. 31–49. Blackwell Scientific Publications, Oxford.

Inman, V. T. and Mann, R. A. (1978) Biomechanics of the foot and ankle. In *Duvries' Surgery of the Foot* (Edited by Mann, R. A.), Chap. 1, pp. 3–21. The CV Mosby Company, St. Louis.

Isman, R. E. and Inman, V. T. (1969) Anthropometric studies of the human foot and ankle. *Bull. Pros. Res.* **11,** 97–129.

Kayano, J. (1986) Dynamic function of medial foot arch. *J. Jpn Orthop. Ass.* **60,** 1147–1156.

Ker, R. F., Bennett, M. B., Bibby, S. R., Kester, R. C. and Alexander, R. McN. (1987) The spring in the arch of the human foot. *Nature* **325,** 147–149.

Klenerman, L. (1982) Functional Anatomy. In *The Foot and its Disorders* (Edited by Klenerman, L.), Chap. 2, pp. 19–30. Blackwell Scientific Publications, Oxford.

Kuhns, J. G. (1949) Changes in elastic adipose tissue. *J. Bone Jt Surg.* **31A,** 541–547.

Lamoreux, L. W. (1971) Kinematic measurements in the study of human walking. *Bull. Prosth. Res.* **BPR10,** 3–84.

Langelann, E. J. van (1983) Relative talotibial movements and relative tarsal movements. In *A Kinematical Analysis of the Tarsal Joints*, Chap. 11, *Acta Orthop. Scand.* (Suppl.) **204,** 135–265.

Mann, R. A. and Hagy, J. L. (1979) The function of the toes in walking, jogging and running. *Clin. Orthop. Rel. Res.* **142,** 24–29.

Mann, R. A. (1982) Biomechanical approach to the treatment of foot problems. *Foot Ankle* **2,** 205–212.

Mann, R. A. (1986) Biomechanics of the foot and ankle. In *Surgery of the Foot* (Edited by Mann, R. A.), Chap. 1, pp. 1–30, The CV Mosby Company, St Louis.

Manter, J. T. (1941) Movements of the subtalar and transverse tarsal joints. *Anat. Record* **80,** 397–410.

Mochon, S. and McMahon, T. A. (1980) Ballistic walking: an improved model. *Math. Biosci.* **52,** 241–260.

Moore, K. L. (1985) *Clinically Oriented Anatomy*, pp. 396–564. Williams & Wilkins, Baltimore, MD.

Morlock, M. and Nigg, B. M. (1991) Theoretical considerations and practical results on the influence of the representation of the foot for the estimation of internal forces with models. *Clin. Biomechanics* **6,** 3–13.

Munro, C. F., Miller, D. I. and Fuglevand, A. J. (1987) Ground reaction forces in running: a re-examination. *J. Biomechanics* **20,** 147–155.

Nakamura, S., Crowninshield, R. D. and Cooper, R. R. (1981) An analysis of soft tissue loading in the foot—prelim. report. *Bull. Pros. Res.* **18,** 27–34.

Onyshko, S. and Winter, D. A. (1980) A mathematical model for the dynamics of human locomotion. *J. Biomechanics* **13,** 361–368.

Ouzounian, T. J. and Shereff, M. J. (1989) *In vitro* determination of midfoot motion. *Foot Ankle* **10,** 140–146.

Pandy, M. G. and Berme, N. (1988) A numerical method for simulating the dynamics of human walking. *J. Biomechanics* **21,** 1043–1051.

Procter, P. and Paul, J. P. (1982) Ankle joint biomechanics. *J. Biomechanics* **15,** 627–634.

Riegger, C. L. (1988) Anatomy of the ankle and foot. *Phys. Ther.* **68,** 1802–1814.

Robertson, D. G. E. and Winter, D. A. (1980) Mechanical energy generation, absorption & transfer amongst segments during walking. *J. Biomechanics* **13,** 845–854.

Salathé, E. P., Jr, Arangio, G. A. and Salathé, E. P. (1986) A biomechanical model of the foot. *J. Biomechanics* **19,** 989–1001.

Scott, S. H. and Winter, D. A. (1991) Talocrural and talocalcaneal joint kinematics and kinetics during the stance phase of walking. *J. Biomechanics* **24,** 743–752.

Siegler, S., Seliktar, R. and Hyman, W. (1982) Simulation of human gait with the aid of a simple mechanical model. *J. Biomechanics* **15,** 415–425.

Siegler, S., Chen, J. and Schneck, C. D. (1988) The three-dimensional kinematics and flexibility characteristics of the human ankle and subtalar joints—Part1: kinematics. *Trans. ASME* **110,** 364–373.

Snijders, C. J., Snijder, J. G. N. and Phillpers, M. M. G. M. (1986) Biomechanics of hallux valgus and spread foot. *Foot Ankle* **7,** 26–39.

Soames, R. W. (1985) Foot pressure patterns during gait. *J. biomed. Engng* **7**, 120–126.
Steinbach, H. L. and Russell, W. (1964) Measurement of the heel-pad as an aid to diagnosis of acromegaly. *Radiology* **82**, 418–423.
Stott, J. R. R., Hutton, W. C. and Stokes, I. A. F. (1973) Forces under the foot. *J. Bone Jt. Surg.* **55B**, 335–344.
Stokes, I. A. F., Hutton, W. C. and Stott, J. R. (1979) Forces acting on the metatarsals during normal walking. *J. Anat.* **129**, 579–590.
Thompson, D. E. (1988) The effects of mechanical stress on soft tissue. In *The Diabetic Foot* (Edited by Levin, M. E. and O'Neal, L. W.), Chap. 6, pp. 91–103. The C. V. Mosby Company, St. Louis.
Tietze, A. (1921) Ueber den architektonischen aufbau des bindegewebes in der bindegewebes in der menschlichen fusohle. *Bruns' Beiträ ge zur Klinischen Chirurgie* **123**, 493–506 (Reprinted as: Concerning the architectural structure of the connective tissue in the human sole. *Foot Ankle* **2**, 252–259, 1982.)
Valiant, G. A. (1984) A determination of the mechanical characteristics of the human heel pad *in vivo*. Ph.D. thesis, Pennsylvania State University, Pennsylvania.
Wanivenhaus, A. and Pretterklieber, M. (1989) First tarsometatarsal joint: anatomical biomechanical study. *Foot Ankle* **9**, 153–157.
Winter, D. A., Quanbury, A. O., Hobson, D. A., Sidwall, H. G., Reimer, G., Trenholm, B. G., Steinke, T. and Shlosser, H. (1974) Kinematics of normal locomotion—a statistical study based on t.v. data. *J. Biomechanics* **7**, 479–486.
Winter, D. A. (1990) *Biomechanics of Human Movement*. Wiley, New York.
Wyss, U. P., McBride, I., Murphy, L., Cooke, T. D. V. and Olney, S. J. (1990) Joint reaction forces at the first mtp. joint in a normal elderly population. *J. Biomechanics* **23**, 977–984.

APPENDIX

THREE-POINT DECOMPOSITION

The decomposition of the load acting on the force plate could be determined if less than four loading sites contacted the force plate. Three loading sites with forces F_1, F_2 and F_3, have coordinates X_1 and Z_1, X_2 and Z_2, and X_3 and Z_3, respectively. The location, X_t and Z_t, and the force, F_t of their combined effects are related by

$$X_t = \frac{\sum X_i F_i}{F_t} \tag{A1}$$

$$Z_t = \frac{\sum Z_i F_i}{F_t} \tag{A2}$$

and

$$F_t = \sum F_i, \quad \text{where } i = 1, 2, 3. \tag{A3}$$

The coordinates, X_i and Z_i, of the three loading sites were determined from the chalked footprint, while the force plate recorded the location, X_t and Z_t, and the force, F_t. Inverse solution of the three equations for each frame of data estimated the force supported at each loading site. This technique was often used when the first and second metatarsals and the first toe landed on the force plate.

TWO POINT DECOMPOSITION

The solution of equations (A1)–(A3) was overdefined when only two metatarsal heads landed on the force plate. Initial analysis of the data showed that the location of the center of pressure under a metatarsal would move slightly along the long axis of the metatarsal. The equation

$$Z_i = mX_i + b \tag{A4}$$

was created to represent the movement of the loading site along the longitudinal axis of each metatarsal. m and b were solved using the average slope of the lines joining the two metatarsal heads on the force plate with their respective toes. This additional equation for the two-point conversion merely allowed a better separation of the loads between the metatarsal heads as compared to the three-point conversion. This technique was often used when the first and second metatarsals or the fourth and fifth metatarsals landed on the plate.

Only a few collected trials recorded the third metatarsal head with less than three other loading sites. Its load was usually estimated by subtracting the averaged loads of the other metatarsals from trials where three or more metatarsals landed on the force plate.